Astronomy Reports, Vol. 48, No. 10, 2004, pp. 853–870. Translated from Astronomicheskiĭ Zhurnal, Vol. 81, No. 10, 2004, pp. 938–955.

A Comparative Analysis of Zebra-Pattern Structures at Frequencies from 20 to 7000 MHz

G. P. Chernov

Institute of Terrestrial Magnetism, the Ionosphere, and Radio Wave Propagation, Troitsk, Russia

Received January 5, 2004; in final form, March 15, 2004

Abstract—A joint analysis of several recent solar type IV radio outbursts with zebra structures and fiber bursts in their dynamical radio spectra is carried out using all available ground-based and satellite data (Yohkoh, SOHO, TRACE). Zebra structures and fiber bursts were observed at frequencies from 20 to 6500 MHz. The main relative spectral parameters and degree of circular polarization of the zebra structures and fiber bursts are nearly the same. The relative width of the zebra structures varies only slightly with frequency ($\approx$0.003–0.005); the radio emission is radiated in the ordinary mode. New data on centimeter-wavelength zebra structures and fiber bursts testifies that they are analogous to similar structures observed at meter wavelengths. A double-plasma-resonance model for the zebra structures based on the observational dependences for the electron density and magnetic field yields a frequency dependence for the frequency separation between stripes that does not agree with the observations. Fine structure was observed together with the rise into the corona of new, hot magnetic loops, in which instabilities associated with high-frequency and low-frequency plasma waves develop. The frequency range of the fine structure in the dynamical spectra is probably determined by the extent of these new loops in the corona. The continuous transition of the fiber bursts into zebra structures and vice versa testifies to a single origin for these two structures. All the main properties of the stripes in emission and absorption can be explained if they are associated with interactions between electrostatic plasma waves and whistlers. It is possible to obtain realistic values for the magnetic-field strength of $B \approx 160$ G at a plasma level of about 3 GHz in this model. © *2004 MAIK "Nauka/Interperiodica".*

1. INTRODUCTION

Stripes of emission and absorption in the form of the more or less regular zebra-pattern structures or of fiber bursts with an intermediate frequency drift against the continuum emission of type IV radio outbursts at meter or decimeter wavelengths were first classified and studied more than 20 years ago [1, 2]. More recent 2.6–3.8 GHz observations with high resolution (10 MHz in 8 ms) using the new spectrograph of the Beijing Astronomical Observatory testify that this type of fine structure displays the same variety at centimeter wavelengths as well [3].

The interpretation of this complex fine structure has always lagged somewhat behind the detection of new, even more varied observational phenomena. However, the generally accepted mechanism for the radio emission of fiber bursts is interactions between electrostatic plasma waves (l) and whistlers (w), both excited by the same population of fast electrons, which has a conical velocity distribution, with the ordinary waves (t) freely escaping: $l + w \rightarrow t$ [4].

The development of the theory of the zebra-pattern structures has been much more complicated; more than ten different models have been proposed, most of them including some role by the emission of electrostatic plasma waves at the double plasma-resonance frequency [4–7]:

$$\omega_{UH} = (\omega_{Pe}^2 + \omega_{Be}^2)^{1/2} = s\omega_{Be}, \qquad (1)$$

where ω_{UH} is the upper-hybrid frequency, ω_{Pe} is the electron plasma frequency, ω_{Be} is the electron cyclotron frequency, and s is the harmonic number. The model that best describes the observations and the conditions in the corona is the model of [7], which is based on unsaturated electron-cyclotron maser emission by electrons with a conical distribution.

However, all these theoretical models developed to explain the zebra structures encounter a number of difficulties.

(1) Irregular structure in the stripes is often observed, although the frequency separations between the zebra-pattern stripes Δf_s should be approximately equal to the electron cyclotron frequency (depending on the relationship between the density and magnetic-field scale heights), and should decrease smoothly with height in the corona. Estimates of Δf_s are presented in [5] for the case when the magnetic-field scale height is much larger than the

1063-7729/04/4810-0853$26.00

electron-density scale height, $L_B \gg L_N$; i.e., when $\Delta f_s \approx f_{Be}$.

(2) The magnetic fields derived based on Δf_s always turn out to be so low that it is difficult to obtain $\beta \approx (v_s/v_A)^2 \ll 1$ for this plasma parameter (the obvious value for a magnetic trap above an active region, where v_s and v_A are the sound speed and the Alfven speed, respectively). This has led many authors to adopt the opposite relationship between the scale heights, $L_B \ll L_N$, but this does not solve this problem, since the real relationship between the two scale heights remains unknown.

(3) Nearly all the models are devised to explain stripes in emission, although stripes predominantly in absorption are also sometimes observed.

(4) All the models assume the important property that the electrons have a conical velocity distribution. This distribution also generates whistlers, and the interaction of these whistlers with fast particles cardinally changes the velocity distribution—the transverse anisotropy is decreased, and bunching of the longitudinal velocities arises.

In addition, the main spectral properties and radio polarizations of the zebra stripes and fiber bursts coincide, which suggests that these two structures are created by a single mechanism, based on the merging of plasma waves and whistlers, but with different conditions for instability of the whistlers.

An entire magnetic trap is filled by periodic wave packets made up of whistlers excited by a conical distribution of fast electrons at the cyclotron resonance:

$$\omega_w - k_{||} v_{||} - s\omega_{Be} = 0, \qquad (2)$$

where ω_w is the whistler frequency, $k_{||}$ is the whistler wave number, and $v_{||}$ is the velocity of the fast electrons along the magnetic field.

Depending on the form of the distribution function, instability develops either for the normal Doppler effect ($s = +1$), when whistlers propagate toward fast particles along magnetic-field lines, leading to the formation of a fiber burst, or in an anomalous resonance [$s = -1$ in (2)], when the whistlers propagate toward fast particles at a large angle to the magnetic field, forming zebra stripes with a different frequency drift [8–10]. The rapid periodicity of the whistler instability is associated primarily with the quasi-linear nature of the instability (the scattering of whistlers on fast particles), which leads to periodic disruptions of the instability of the electrostatic waves in the volume of the whistler wave packet. This effect gives rise to bands of absorption that accompany both fiber bursts and zebra stripes of emission [11]. Whistlers can contribute to the formation of bands of emission and absorption as a result of their interaction with plasma waves at both the sum and the different frequencies, $\omega_l \pm \omega_w = \omega_t$ [9, 12, 13].

The unsatisfactory lack of a single generally accepted theory for the zebra-pattern structure has unfortunately stimulated many authors to devise new versions of models based on the double plasma resonance [14, 15]. Ledenev *et al.* [14] suggest that the magnetic field falls off with height in the corona much more rapidly than the density. Under the assumption that radiation is emitted at the second harmonic, ω_{UH}, they obtained more realistic values for the magnetic field, comparable to those obtained in [3] for whistler models. However, the zebra structure is usually strongly polarized (it only very rarely has low polarization), which excludes the possibility that this emission is radiated at the second harmonic. Therefore, the B values turn out to be overestimated by more than a factor of two; in addition, the harmonic number s was chosen arbitrarily.

In an attempt to remove the problem of the low magnetic field that is implied by assuming that the radiation is associated with the double plasma resonance, LaBelle *et al.* [16] proposed a new theory for zebra structures based on the radiation of auroral "choruses"—magnetospheric outbursts detected at ground-based stations at frequencies of 2–4 MHz, which have fine structure similar to that of the zebra-pattern structure. This model proposes that the radiation is emitted in the cyclotron-maser Z mode (by analogy with [7]). Although the upper-hybrid-frequency Z-mode radiation itself does not emerge from the source, this radiation can be transformed into ordinary-mode (O-mode) radiation at discrete frequencies (the eigenharmonics) in the presence of density inhomogeneities on the corresponding scales. These discrete frequencies arise due to the quantization in the conditions of the eiconal when the wave passes through an Ellis window for the corresponding azimuthal (m) and radial (n) quantum numbers in the eiconal conditions. The Z mode can be generated in a point source at one level of the double plasma resonance [$s = \text{const} = 2$ in (1)]. The main difference and advantage of this model is that it can explain the formation of a large number of harmonics (up to 100) with a small frequency separation $\Delta f_s \approx 0.01 f_{Be}$. LaBelle *et al.* [16] estimated the degree (<10%) and size (1–100 m) of the density inhomogeneities. Such inhomogeneities could be created by dispersional ion–acoustic waves. However, LaBelle *et al.* [16] do not discuss one important aspect of the problem—the time dependence of the eigenharmonics (the dynamics of the zebra-pattern structure); they only mention the possibiity that the inhomogeneities could be stable over ~10 s. They likewise do not discuss the conditions for the excitation of the ion–acoustic waves and the main condition that

the electron temperature greatly exceed the ion temperature ($T_e \gg T_i$). In addition, the summing of the contributions of numerous inhomogeneities (created by propagating ion–acoustic waves) should lead to blending of the stripes into the continuum. The simultaneous appearance of fiber bursts against the zebra structure is likewise not considered. We will discuss other discrepancies with the observations in Section 3 below.

Observations of zebra structure at the harmonic frequencies 1700 and 3400 MHz were first discussed in [17]. However, the absence of polarization information and the lack of similarity between the zebra structures at the harmonic frequencies casts doubt on the reality of this harmonic structure.

Observations of fine structures have been considerably expanded in recent years, leading to the discovery of new effects in the zebra structure. Analyses of new events now usually include a more complete study of flare processes contributing to the X-ray emission (Yohkoh/SXT) and the ultraviolet lines (SOHO and TRACE). It is therefore important at this stage to identify new properties of the fine structure observed at various frequencies and analyze them in the context of various theoretical models; this is the goal of the current paper.

Zebra-pattern structures and fiber bursts are sometimes not observed simultaneously over a wide range of frequencies spanning decameter to decimeter wavelengths. On the contrary, the frequency bands occupied by the fine structure associated with a single event are usually $\leq$50 MHz at meter wavelengths and several hundreds of MHz at decimeter wavelengths. We will compare the relative parameters of the zebra structures at different frequencies and attempt to answer the question of why these frequency bands are so narrow. We analyze four radio outbursts displaying fine structure at meter wavelengths (the events of May 2, 1998, July 28, 1999, September 23, 1998, and October 25, 1994) and two such outbursts at centimeter wavelengths (October 29, 2000 and April 21, 2002).

2. DESCRIPTION OF THE EVENTS

Several major type IV radio outbursts displaying fine structure in the form of emission and absorption stripes (zebra-pattern structure and fiber bursts) were observed with several radio spectrographs [ARTEMIS (Nancay), 100–500 MHz; IZMIRAN (Institute of Terrestrial Magnetism, the Ionosphere, and Radio Wave Propagation), 25–270 MHz; PHOENIX-2, 220–549 MHz; Nancay, 20–70 MHz; Potsdam (Tremsdorf), 40–800 MHz; Beijing Astronomical Observatory, 2.6–3.8 and 5.2–7.6 GHz], as well as with the Nancay radioheliograph and the Trieste Astronomical Observatory polarimeter at 237, 327, and 408 MHz. We also used all available higher-frequency data for the analysis, including images in UV lines obtained with the SOHO and TRACE satellites and in the soft X-ray with Yohkoh/SXT. This enabled us to carry out a comparative analysis of the zebra structures over a wide range of frequencies from 30 to 6500 MHz.

2.1. Event of May 2, 1998

Zebra-pattern structures were first observed for event of May 2, 1998 at low frequencies between 22–46 MHz (Fig. 1). The radio event was simultaneous with a large 3B X1.1 flare at 13:30–13:42–15:13 UT in the active region NOAA 8210, with coordinates S15W15. The SOHO LASCO telescope detected a major halo-type coronal mass ejection (CME) extending to 26 $R_\odot$.

The radio event included a large group of type III outbursts, two type II outbursts, and type IV continuum radiation. A global dynamical spectrum is presented in [18]. The maximum energy release in the corona occurred at the heights where the decimeter radiation was generated (22 000 s.f.u. at 606 MHz), but the event continued into interplanetary space, expressed via a type II and very weak type III outburst.

Zebra-pattern structure was observed over approximately three minutes, in the form of structure in the flare continuum after the strong type II and type III outbursts. The dynamical spectrum shown in the upper panel in Fig. 1 shows that the zebra structure consists of numerous fragments of stripes with various frequency drifts. The most substantial long fragment resembles a narrow-band braid of stripes (or short-time-scale fiber bursts) with a constant frequency drift. This main braid of fibers, which lasted about two minutes, forms the low-frequency boundary of all the zebra-pattern fragments. These fragments also form braids of fibers occupying various frequency bands at higher frequencies.

The frequency drift of the main braid is approximately -0.13 MHz/s near 37 MHz, which corresponds to a speed for the propagation of the excitation in the outer layers of the corona of about 2200 km/s (if we use a double Newkirk model for the electron density). The frequency-drift rate is approximately -0.04 MHz/s, which corresponds to a motional velocity of 700 km/s. We should note two more important properties of the main braid: its frequency width increased from 0.25 MHz at 43 MHz to 0.8 MHz at 22 MHz, accompanied by an appreciable decrease in the left-circular polarization.

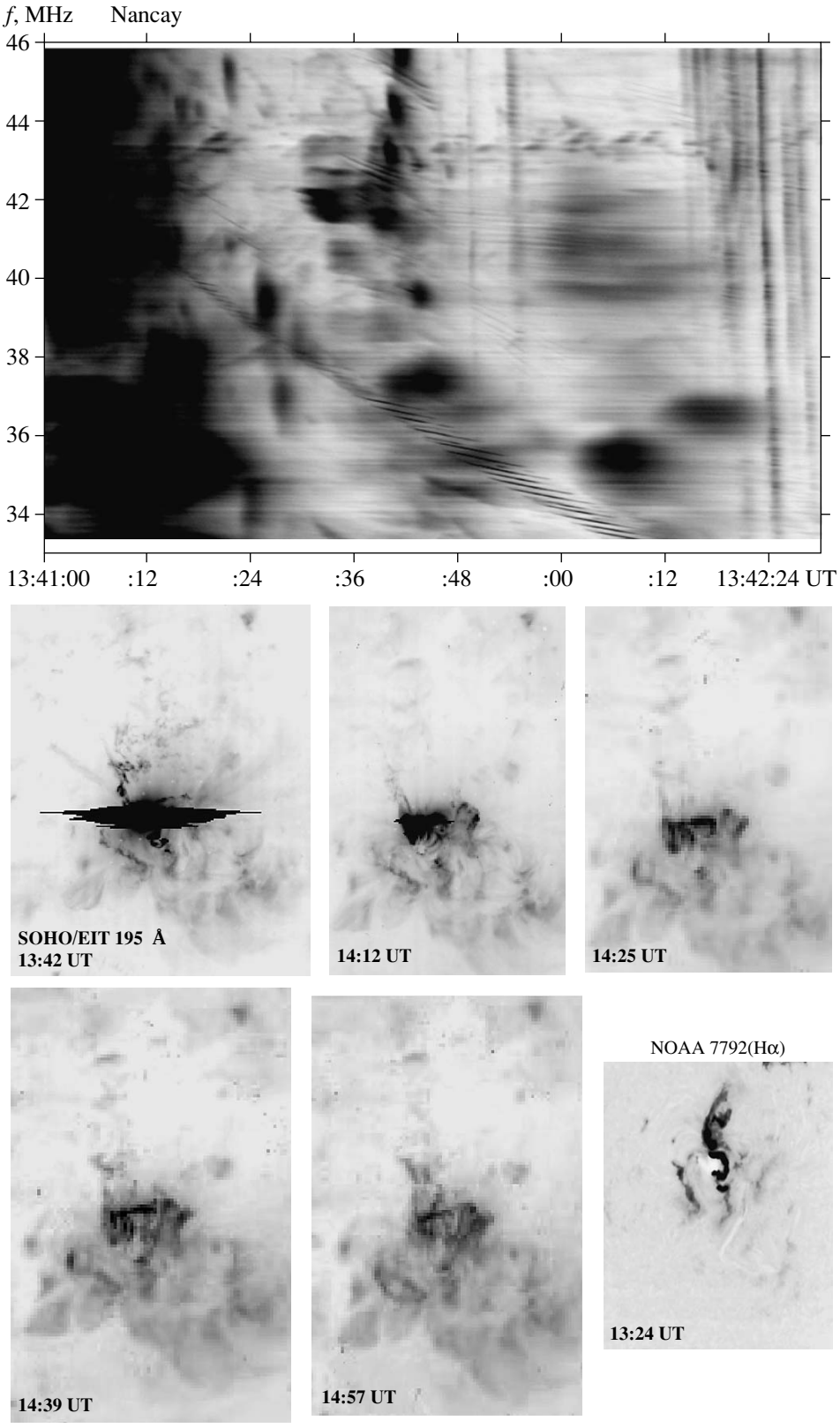

Fig. 1. Event of May 2, 1998. The top panel shows the dynamical spectrum obtained using the DSP decameter spectropolarimeter of the Nancay Observatory (the time resolution is 0.05 s). The lower panels show the development of the outburst in the 195 Å EUV line (SOHO/EIT) and the Hα emission in the active region (NOAA 7792).

The width of the frequency bands for individual stripes of emission was approximately the same for all the zebra-structure fragments, $\Delta f \approx 0.08$ MHz, with the relative width of these bands being $\Delta f/f \approx 0.0024$. However, the frequency separations between the stripes of emission were appreciably different in different fragments ($\Delta f_s \approx 0.08$–0.17 MHz), and the short-time-scale stripes within the main braid are not strictly periodic in frequency. In some fragments, a frequency shift toward lower frequencies is observed between an emission stripe and the neighboring absorption stripe, Δf_{ea}. This shift is approximately equal to Δf.

The radio emission of all components of the type II and type III outbursts was essentially unpolarized, while the main braid displayed strong left-circular polarization. Other fragments of the zebra structure displayed moderate left-circular polarization, while still others even displayed moderate right-circular polarization.

Two-dimensional NRH images of the 164 MHz radio sources obtained show four radio sources above active region NOAA 8210. The complex behavior of the polarization of the fine structure may indicate that different radio sources are located in regions with different magnetic polarities.

The lower part of Fig. 1 displays the evolution of the flare in the 195 Å EUV line (five frames from SOHO/EIT MPEG film), while the fifth lower panel shows the onset of the Hα flare. We can see in this last panel that a helmetlike ejection has already formed over the sigmoid flare ribbon by 13:24 UT. The continuation of this ejection is clearly visible in the first 195 Å frame, which corresponds to the maximum of the flare (13:42 UT). Each subsequent frame contains new fragments of ejected material in projection onto the disk. It is obvious that, after the CME, the energy release proceeded in a vertical current layer, as a magnetic structure with magnetic islands was established.

2.2. Event of July 28, 1999

The radio event consisted of a prolonged type IV outburst with zebra structure in the interval 08:15–10:30 UT, associated with a modest 1B M2.3 flare with its maximum at 08:14 UT in the active region NOAA 8649 (S15E03). The flare was accompanied by a halo-type CME at 09:06 UT. We can identify three main intervals in which fine structure was displayed: 08:15–08:30 UT, in the impulsive phase, 08:50–09:25 UT, at the maximum, and 10:15–10:30 UT, in the decay phase. In the first two intervals, the zebra-pattern structure is chaotic on short time scales (less than one minute) in narrow frequency bands (of 50–150 MHz) between 200 and 1500 MHz. In the decay phase, the zebra structure is displayed nearly continuously at 300–400 MHz.

The upper left panel in Fig. 2 shows the zebra structure at the end of the impulsive phase observed at IZMIRAN at 200–270 MHz. The upper right panel presents the zebra structure obtained on the Phoenix-2 specrograph at 320–385 MHz during the decay phase. We can see in the left panel that the zebra stripes drift toward high frequencies, as is often observed. The right panel displays various drifts, but the overall tendency is for the zebra stripes to drift toward lower frequencies, and the stripes in this part of the spectrum resemble fiber bursts.

A common feature of the stripes observed in these two frequency bands is the presence of absorption relative to the mean continuum level at the low-frequency edge of the emission stripes, as is confirmed by the left- and right-circular polarization profiles for 237 MHz (left) and 327 MHz (right) presented in the central panels of Fig. 2 (data of the Trieste Astronomical Observatory). The degree of left-circular polarization was initially moderate (30–40%), becoming stronger at the end of the event (60–80%). The dips in intensity in the absorption bands were 20–30% of the mean continuum level.

After the maximum of the event at about 08:55 UT, unusual stripes of emission with absorption on both the low-frequency and high-frequency sides began to appear, together with individual bands of pure absorption. Further, after 10:19 UT, nearly all the zebra stripes and individual fiber bursts had their absorption on the opposite (high-frequency) edge. The stripes displayed a continuous variation of the frequency drift in this interval, from negative to positive, in the form of cascades of U flares. In this case, the zebra stripes made a continuous transformation into fiber bursts and vice versa. Two such cascades are visible in the right-hand spectrum in Fig. 2.

The three lower panels in Fig. 2 show the evolution of the flare at 195 Å displayed by SOHO/EIT data. The flare began above a neutral magnetic-field line, with zebra-pattern structure observed at 08:15 UT simultaneous with the rise of a new loop (toward the southwest in projection), shown by the arrow in the left panel. This loop continued to rise until 08:25 UT, and the NRH data show that the 327 MHz radio source was located above this loop. The position of this source is marked by a white plus in the central panel.

At the time of the event's maximum, new bright flare centers were ignited to the west of the main flare. In the decay phase, a new loop began to rise above these centers, and the radio sources that appeared during the decay-phase zebra structure were located above this new loop; the 327 MHz and 164 MHz

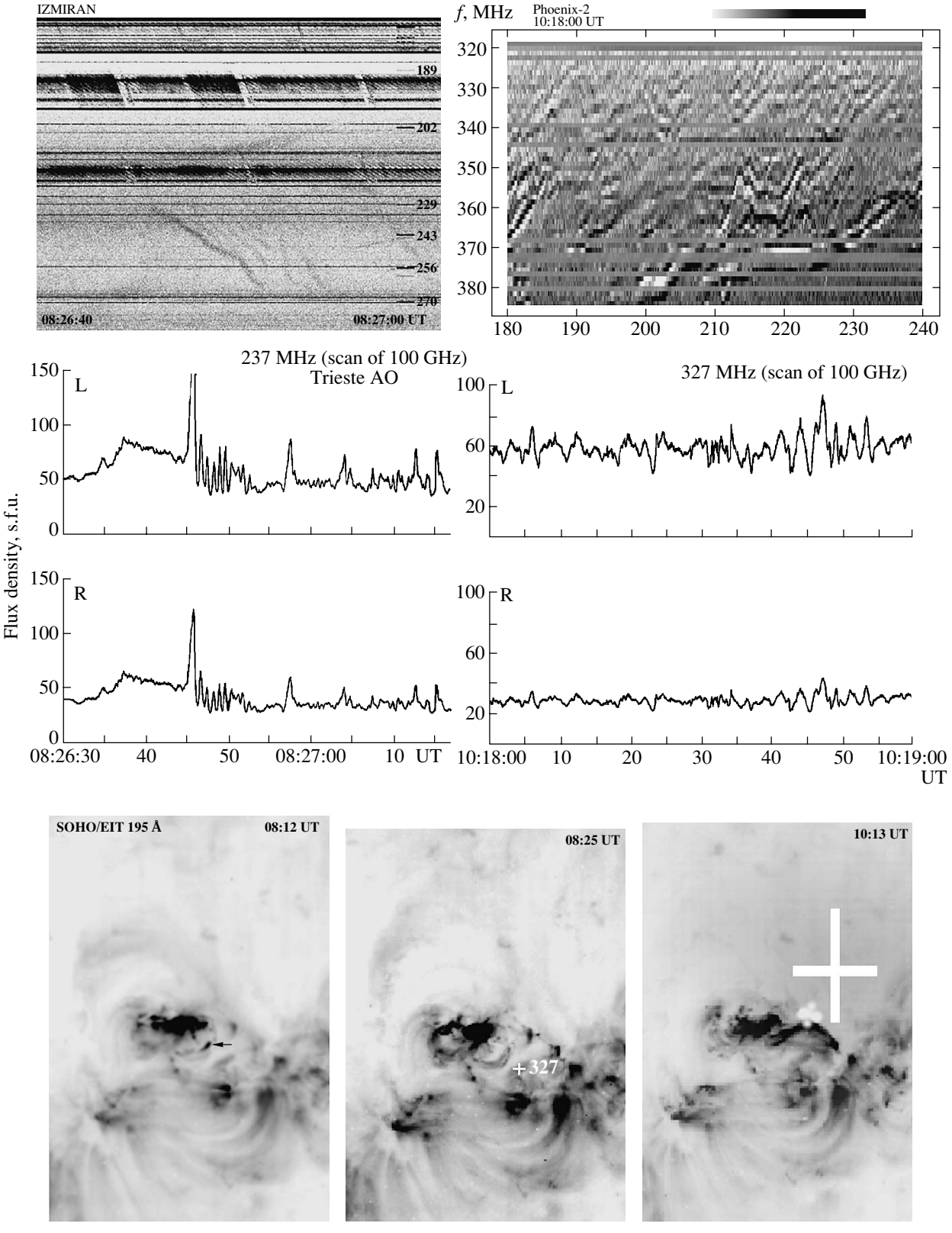

Fig. 2. Event of July 28, 1999. The upper panel shows two spectra of the zebra structure during two active periods at 08:26 UT (left, the IZMIRAN spectrograph,189–270 MHz) and 10:18 UT (right, the Phoenix-2 spectrograph, 320–385 MHz). The central panels show temporal profiles of the L and R chanels of the Trieste Astronomical Observatory polarimeter at 237 and 327 MHz. The lower panels show the evolution in the 195 Å EUV line (SOHO/EIT). The arrow in the left frame shows the rise of a new loop. The white pluses in the other frames show the positions of the centers of the radio sources at 327 MHz (small) and 164 MHz (large).

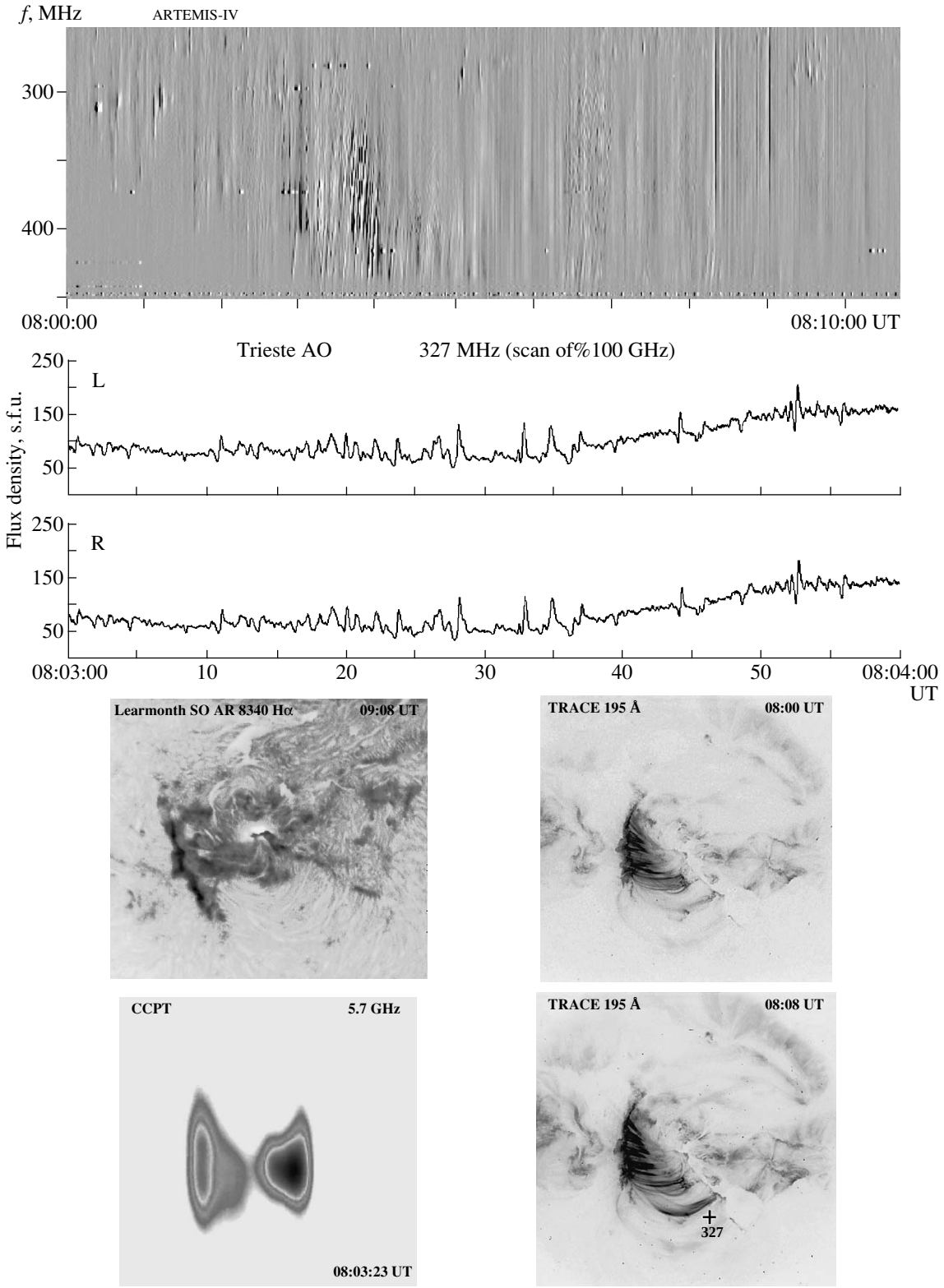

Fig. 3. Event of September 23, 1998. The upper panel shows the fine structure displayed between 08:00 and 08:10 UT at 250–450 MHz (the ARTEMIS-IV spectrograph, Greece). The next panel presents time profiles of the L and R channels of the Trieste Astronomical Observatory polarimeter at 327 MHz, which show weak left-circular polarization. The lower set of panels present the development of the Hα flare (upper left; Learmonth Solar Observatory), two EUV 195 Å frames, which show numerous hot loops between two parts of the neutral line (right; TRACE), and the radio brightness distribution at 5.7 GHz (lower left; CCPT). The position of the center of the radio source at 327 MHz (NRH) is indicated by the cross above the new loop at 08:08 UT.

radio sources are marked by the small and large white pluses in the central and right panels of Fig. 2.

2.3. Event of September 23, 1998

According to Solar Geophysical Data (SGD), a 3B M7.1 flare began at 06:40 UT in the active region NOAA 8340 (N18E09), reaching its maximum at 07:13 UT. The radio event was observed from 06:52–11:00 UT, and included a type II outburst (06:52–07:02 UT) and a prolonged type IV outburst with several maxima. Zebra structure was observed in the interval 08:00–08:10 UT. In the spectrum in the upper panel of Fig. 3, obtained with the new ARTEMIS-IV spectrograph (Greece) at 250–450 MHz, we can see a fiber burst (08:03–08:04 UT), riblike zebra structure (08:05–08:06 UT), and rapid pulsations in emission and absorption (08:08–08:09 UT). Below the spectrum, a rare property of the fine structure is visible in the 327-MHz polarization profiles obtained at the Trieste Astronomical Observatory: the radiation displayed very weak left-circular polarization. These profiles also show that the dips in intensity in the absorption stripes comprise about 20–30% of the mean continuum level. The zebra structure observed at 08:06–08:07 UT was most pronounced in absorption, and the rapid pulsations observed at 08:08–08:09 UT were also purely in absorption (i.e., they were "sudden reductions").

The evolution of the flare is illustrated in four different panels in the lower part of Fig. 3. A two-ribbon Hα flare was observed over three hours along the eastern and western parts of a neutral line of the magnetic field. The two TRACE 195 Å frames show numerous bright loops that appear (and disappear) betwen these two parts of the neutral line. A new bright loop appeared in the southern part of the flare region at 08:00 UT, and the center of the 327 MHz radio source observed at 08:08 UT (NRH) coincides with this new loop in the 195 Å TRACE frame.

Many aspects of the structure of the radio sources and the fine structure of the radio emission at centimeter wavelengths have been studied in [19, 20]. For our analysis, it is important that the 5.7 GHz radio source observed by the CCPT has a double structure, with the source on the right (which was located near the eastern part of the neutral line and was closest to the position of the meter-wavelength source) being brighter at 08:03 UT (Fig. 3, lower left panel). The dynamics of the 195 Å flare loops (TRACE) are impressive: every few minutes over three hours, new loops were ignited and rose high into the corona. The onset of the type II outburst was accompanied by flare ejections toward the southwest observed in the 1550 Å line (SOHO/ZUMER). Several minutes later, a dark region that can be considered a flare coronal hole (or dimming) formed at the location of this ejection, and was subsequently observable for many hours in the 195 Å line (TRACE).

2.4. Event of October 25, 1994

Beginning at 10:00 UT, the meter-wavelength radio event included a type II outburst at frequencies below 90 MHz, which had drifted to 40 MHz by 10:06 UT, and a brief type IV outburst (flare continuum) with fine structure in the form of periodic type III outbursts between 10:05:18 and 10:08:35 UT and zebra-pattern structure between 10:08:00 and 10:09:00 UT. The upper panel of Fig. 4 shows the dynamical spectrum obtained on the ARTEMIS spectrograph (Nancay Observatory) at 100–500 MHz. The type III outbursts have a very high frequency-drift rate (possibly associated with an enhanced plasma density above the flare region). However, this frequency-drift rate is lower at lower frequencies. The main energy release occurred at meter wavelengths. The maximum flux at 204 MHz was 300–400 s.f.u. between 10:08 and 10:09 UT.

A modest centimeter-wavelength flare (a 49 s.f.u. GRF) was observed over an hour, and an even more prolonged C4.7 soft X-ray (1–8 Å) flare was detected by the GOES-7 satellite. According to SGD 608 II, a modest 1N-magnitude Hα flare began at 09:40 (reaching its maximum at 10:04 UT and its end at 12:36 UT) in active region NOAA 7792 (S09W12). An active dark fiber and system of filaments were also visible above this active region.

Some aspects of the type IV radio outburst, which displayed various source positions outside the active region, are discussed in [21]. In the superposition of the 164 MHz radio source and the soft X-ray (Yohkon/SXT) A1.1 image shown in the lower left panel of Fig. 4, the center of the radio source is located outside the active region. At this same time, the main continuum source coincided with the main flare region in the soft X-ray. Each subsequent X-ray frame contains new bright loops, both inside and outside the main flare region, providing evidence for magnetic reconnection occurring in neighboring loops. Thus, it is likely that the repeated radio flares at 327 and 408 MHz had different circular polarizations. The maximum brightening in soft X-rays occurred at 09:59 UT, before the type II outburst, and at 10:08 UT, during the type III outbursts in the same location, at the center of the active region, above the magnetic-field neutral line. The sigmoid shape of the soft X-ray flare repeats the shape of the neutral line. Manoharan *et al.* [22] suggest that the flare acted as a trigger for large-scale magnetic reconnection.

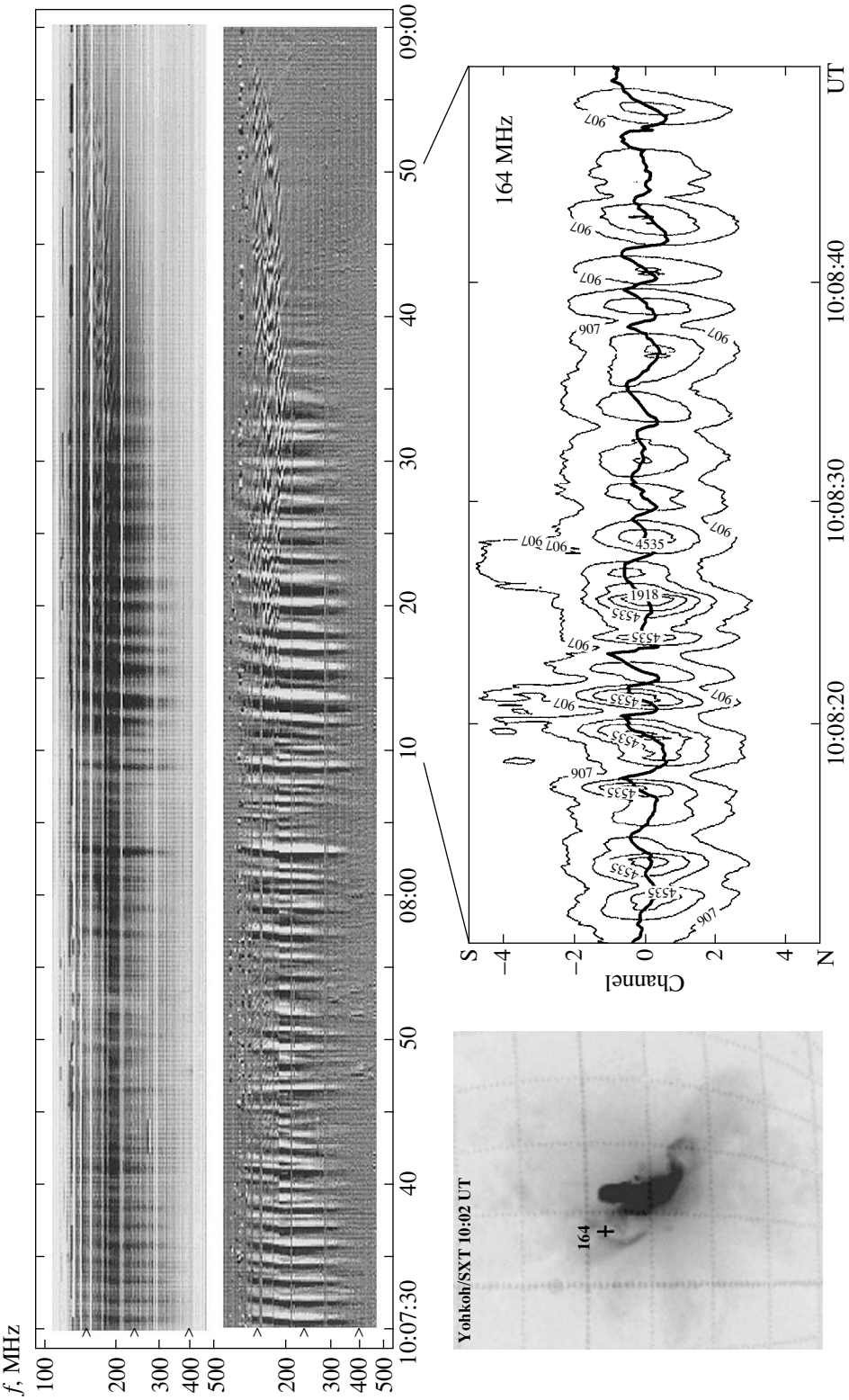

Fig. 4. Dynamical spectrum of the periodic type III outbursts (reminiscent of pulsations) in event of October 25, 1994 over the entire range of the ARTEMIS spectrograph, 100–500 MHz (intensity is shown in the upper spectrum and the derivative of the signal in the lower spectrum), with zebra-pattern structure visible at 135–210 MHz. The lower right panel shows simultaneous S–N contours of the radio brightness distribution at 164 MHz (NRH). The bold line passing through the centers of the sources shows their spatial drift. The lower left panel shows the position of the 164 MHz radio source (marked by a plus) superposed on an X-ray image of the flare (Yohkoh/SXT, the A1.1 thin filter), demonstrating that this radio source is located outside the bright flare region.

In this event, zebra structure was observed at frequencies between 210 and 130 MHz against the background of the type III outbursts, which drifted from 400 to 150–125 MHz (Fig. 4, ARTEMIS data).

We would like to point out certain key features in Fig. 4, which enable us to understand the overall dynamics of the event. The initial frequency of the type III outbursts oscillates between 300 and 450 MHz, with a period that smoothly grows from 10–15 min at the onset to roughly 30–35 min at the end of the series of type III outbursts. This may be associated with slow MHD fluctuations in the region in which the fast particles are accelerated. The low-frequency limit where the drift of the type III outbursts ceases also fluctuates asynchronously with the high-frequency initial frequency: this limit dropped to approximately 125 MHz between 10:08:12 and 10:08:30 UT. A clear sign of a new perturbation is provided by an abrupt break in the frequency drift between 10:07:38 and 10:07:57 UT, with the drift settling at a frequency of 170 MHz. Three seconds later, zebra-pattern structure appears beginning at precisely this frequency and occupying frequencies down to 140 MHz. Over an eight-minute interval, the zebra structure expanded from 130 to 210 MHz, and the type III outbursts gradually disappeared (their intensity and frequency range smoothly decreased). When the zebra structure is most fully developed, at 10:08:17–10:08:24 UT, it is possible to distinguish up to 17 emission stripes, with the frequency separation between the stripes slowly growing from 1.7 MHz at 140 MHz to roughly 2.2 MHz at 170 MHz. The polarization of the radio emission of the zebra structure and the type III outbursts was moderate (25–30%), with the maximum polarization corresonding to the zebra structure without type III outbursts at the end of the eighth minute. The right-circular polarization in the source above the trailing spot of southern polarity corresponds to a predominance of the ordinary wave.

The lower right panel of Fig. 4 shows contours of the one-dimensional S–N radio-brightness distribution at 164 MHz (NRH). The maximum brightness corresponds to the center of a zebra-pattern stripe after approximately 10:08:33 UT or a type III outburst before this time. The solid line passing through the source centers shows the spatial drift of the sources at a fixed frequency. First and foremost, we note that the positions of the sources of type III emission and zebra structure coincide (in both the N–S and E–W directions; i.e., in a disk). It is noteworthy that the type III sources drift in the direction S → N (at the beginning of the spectrum), while the sources of pure zebra structure (at the end of the spectrum) drift in the opposite direction, N → S. In all the zebra-pattern absorption stripes, the drift of the source is the same as for the type III outbursts (for example, at time 10:08:33.4 UT).

The vertical scale for the one-dimensional S–N radio-brightness distributions in Fig. 4 is presented in terms of the number of spatial channels for the Nancay radio interferometer. At 164 MHz at this time, the first channel in the S–N direction corresponds to approximately 3.2′. Therefore, the full widths at half maximum of the sources of both the zebra structure and the type III outbursts are, on average, 1.5 channels (about 4.8′); the maximum spatial-drift rates are $>90\,000$ km/s ($\approx 170\,000$ km/s for the type III outbursts). Since these are projected onto the disk, the real source drift rates will always be $>10^{10}$ km/s (close to the speed of light). Thus, the observed size of the source is essentially the size of the active region, and the observed drift rate can be supplied only by fast (relativisitic) particles. Similar zebra-structure drift rates were obtained earlier for event June 5, 1990 [23].

Let us note another important fact: the zebra structure forms several humps with changing signs of the frequency drift, with the sign changes correlating with changes in the sign of the spatial drift of the source. Negative frequency drift corresponds to the type of drift occurring in type III outbursts, and changes in the sign of the source drift are observed at times when the frequency drift changes sign (for example, at times 10:08:32 and 10:08:36.5 UT). These data enable us to explain the frequency band occupied by the zebra structure in the dynamical spectrum (see the Discussion below).

In interplanetary space, the URAP experiment on the Ulysses satellite detected one type III outburst at 10:10 UT at frequencies below 1000 kHz, due to a beam of electrons accelerated at the onset of the flare.

2.5. Centimeter wavelengths

We selected several dozen cases of zebra-pattern structure and fiber bursts in four events at 2.6–3.8 GHz and one case at 5.2–7.6 GHz. In all cases, the zebra-structure and fiber-burst radiation was strongly polarized near 3 GHz, but weakly polarized at 5.2–7.6 GHz. The most saturated fine structure was observed in the centimeter-wavelength outbursts of April 15, 1998, October 29, 2000, and April 21, 2002. This last event occurred at the limb. Via a comparison of the times when zebra structure was manifest with the positions of radio sources indicated by Nobeyama heliograph observations at 17 GHz and with the development of the flare in the 195 Å line indicated by SOHO/EIT (and SOHO/MDI magnetogram) data for the first two events, it was possible to determine that the ordinary mode dominated in the radiation. Our observations show that

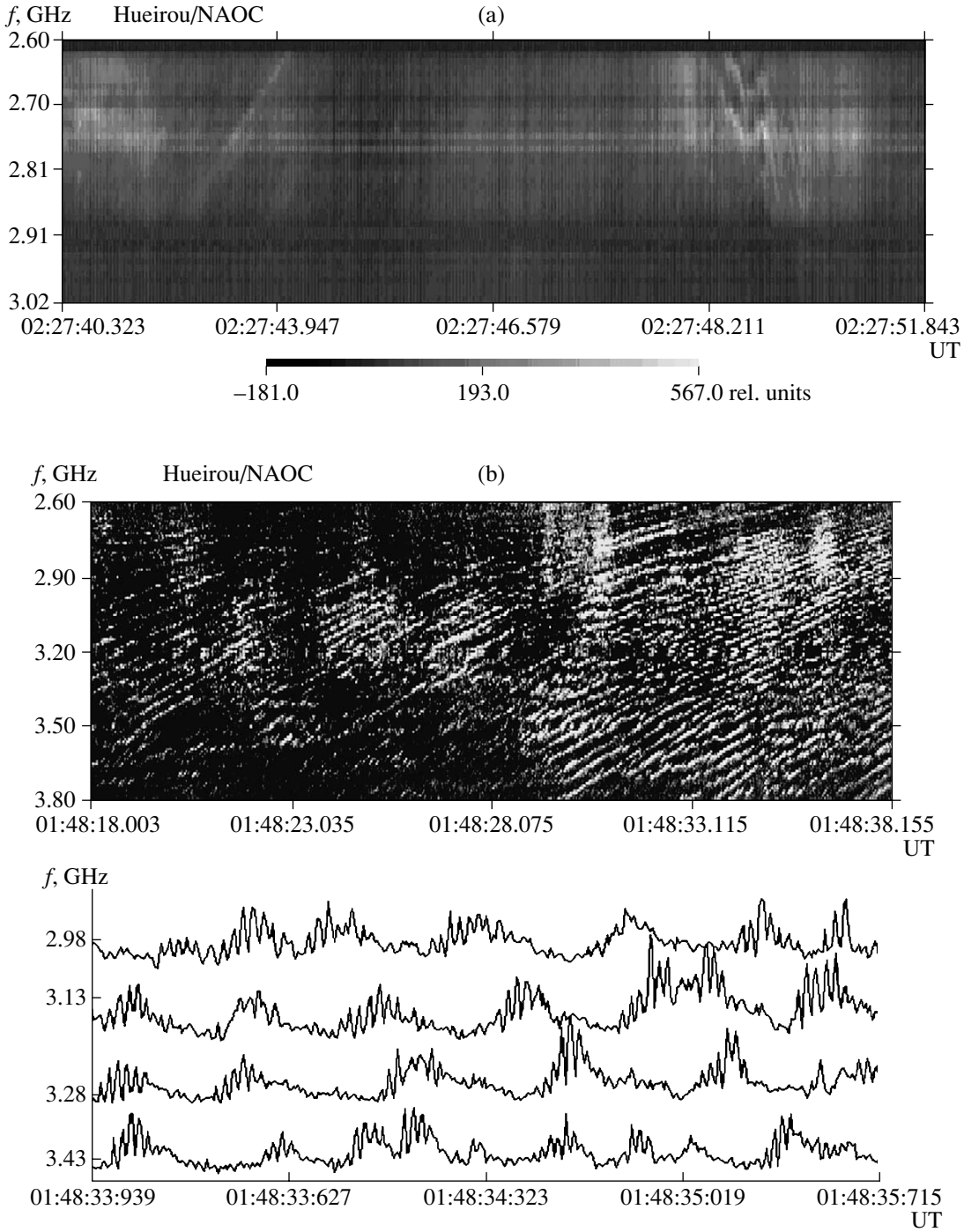

Fig. 5. (a) Zebra structure in a fiber burst in event of October 29, 2000 observed in right-circular polarization by the NAOC spectropolarimeter (Beijing). (b) Zebra structure in event April 21, 2002. The upper panel shows the spectrum in left-circular polarization, in which 34 stripes whose frequency separation grows smoothly with frequency can be distinguished. The lower panel shows profiles of the intensities at four fixed frequencies.

all the variety of zebra structure and fiber bursts known for decimeter and meter wavelengths is also characteristic of events at centimeter wavelengths. Figures 5a and 5b depict the development of zebra structure and fiber bursts in events of October 29, 2000 and April 21, 2002, which were most rich in fine structure. In event of October 29, 2000, series of zebra-pattern structures were present in a pulsating regime for approximately 30 minutes following the maximum of the flare. Each series had a duration of

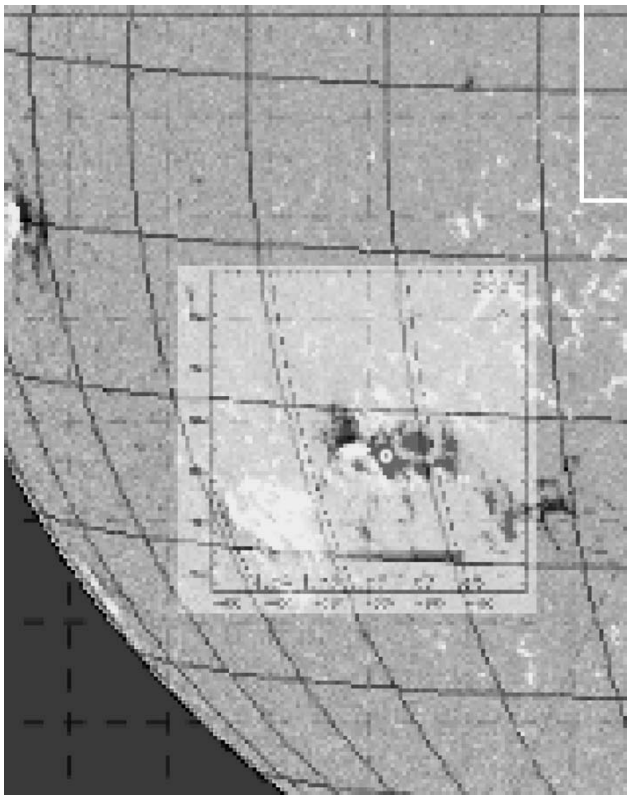

Fig. 6. Position of the center of the radio source in event of October 29, 2000 at 17 GHz, shown by a light circle against the background of the S-polarity magnetic field recorded on the SOHO/MDI magnetogram, on which the radio brightness distribution derived from the Nobeyama radio-heliograph data is superimposed.

about 2–3 s and three to five zebra-pattern stripes, with various frequency drifts; a fiber burst with a constant negative drift sometimes accumulated in the zebra structure (Fig. 5a).

Event of October 29, 2000 was associated with a 2B M4.4 Hα flare in the active region NOAA 9209 (S25E35). The position of the center of the radio source at 17 GHz is shown in Fig. 6 by a light circle against the background of the S-polarity magnetic field detected by the SOHO/MDI magnetogram, on which the radio-brightness distribution obtained using the Nobeyama Radio Heliograph is superimposed. The radio source is located above the S-polarity magnetic field, so that right-circular polarization corresponds to the O mode of the radio emission.

In event of April 21, 2002 (Fig. 5b), up to 34 zebra-pattern stripes can be distinguished in the spectrograph band, 2.6–3.8 GHz, with a barely perceptible growth in the frequency separation between the stripes from 27 MHz at 2.8 GHz to 43 MHz at 3.7 GHz. The moderate degree of left-circular polarization increased appreciably with time and frequency, even within a single series of zebra structures with a duration of 20 s.

A detailed analysis of the multi-channel time profiles shows that the radiation level in the dark bands between bright stripes can be lower than the background level for the flare (see the profiles at several fixed frequencies in the lower panel of Fig. 5b). Thus, the presence of dark stripes is not associated only with an absence of bright stripes (in emission), but with genuine absorption of the centimeter-wavelength background. In this connection, the main characteristic of the zebra structure is the frequency separation between neighboring peaks in emission and absorption, Δf_{ea}, rather than the frequency separation between stripes of emission, Δf_s. While the latter is determined (for example, in double-plasma-resonance models for the zebra structure) by mutual variations of the plasma frequency and electron-gyrofrequency harmonic with height in the corona, Δf_{ea} is determined directly by the mechanism that forms the stripes in emission and absorption. Despite the variety in the zebra-pattern stripes, the mean value of $\Delta f_s/f$ for all the events is about 60–80 MHz at 2.6–3.8 GHz, while the mean value of the parameter $\Delta f_{ea} \approx 30$–40 MHz for both zebra structure and fiber bursts. Fiber bursts do not always display regularity in frequency, and most often each fiber burst is manifest as a weak outburst; but the parameter Δf_{ea} testifies to a related origin for the bands associated with zebra structure and fiber bursts.

The main parameters of the zebra structure and fiber bursts for five events are collected in the Table. The parameters $\Delta f_s/f$ and $\Delta f_{ea}/f$ grow with frequency, clearly in connection with the growth of the magnetic field. The parameter $\Delta f_b/f$ decreases with frequency, which corresponds to a decrease in the size of the radio sources in the lower corona. Only the quantity $\Delta f/f$ remains nearly constant. In four events, the radio fine structure corresponded to the ordinary mode.

3. DISCUSSION

Four radio events with zebra structure and fiber bursts at meter wavelengths were closely associated with flares of various magnitudes or type II outbursts (due to shocks in and CMEs), but, in all the events, the maximum energy release occurred high in the corona as a result of magnetic reconnection. The polarization of the radio emission was moderate in all events, and corresponded to the ordinary mode in three cases.

Parameters of the zebra structure in five events

Date Time (UT)	f, MHz Frequency, MHz	Flare Coordinates	$\Delta f_s/f$	$\Delta f_{ea}/f$	$\Delta f_b/f$	$\Delta f/f$	Magnetic polarity	Sign of the polarization Mode
1998-05-02	35	3B X1.1	0.0036	0.0024	0.88	0.0035	S(N)	LR
14:41	20–70	S15, W15						?
1994-10-25	175	1N C4.7	0.015	0.006	0.4	0.0049	S	R
10:08	100–500	S09W12						O
1999-07-28	360	1B M2.3	0.014	0.006	0.22	0.0054	N	L
08:15	45–520	S15E03						O
1998-09-23	360	3B M7.1	0.064	0.032	0.3	0.014	N	L
08:00	100–700	N18E09						O
2000-10-29	3000	2B M4.4	0.033	0.015	0.16	0.0059	S	R
02:20	1000–3800	S25E35						O

Note: $\Delta f_s/f$ is the relative frequency separation between the zebra stripes; $\Delta f_{ea}/f$ is the relative frequency separation between stripes in emission and absorption; $\Delta f_b/f$ is the relative frequency bandwidth of the fine structure in the spectrum; $\Delta f/f$ is the relative instantaneous frequency bandwidth for a single stripe of emission.

3.1. Event of May 2, 1998

The braids of fibers shown in Fig. 1 strongly resemble similar structures observed earlier at higher frequencies (200–250 MHz) and discussed in [9, 24, 25]. However, these latter structures were repeated multiple times over the entire decay phase of a flare (over more than an hour). They are associated with whistler instabilities in a small magnetic trap that has formed between shock fronts moving away from a magnetic-reconnection X point during the prolonged process of reestablishing the magnetic structure after a CME.

We can see ejections in various directions in five frames in the 195 Å line (SOHO/EIT), but two of these are most prominent: one toward the north from the main flare and the other toward the southwest (a slowly moving front). This is suggestive of a perturbation (shock front) moving toward the observer. It may be that the source of the fiber braids is associated with this shock front, and is located in a narrow trap between the front and the leading edge of a CME: the braids are observed over only three minutes during the type II outburst, and the frequency drift of the main braid is determined by the motion of the shock front with a speed of $\approx$2200 km/s.

Fast particles accelerated in the shock front were captured in this narrow trap (with a width of several thousand kilometers). As a result of the "bounce" effect—the motion of these particles between the two maxima of the magnetic field (in the shock front and the leading edge of the CME)—a conical velocity distribution was formed, giving rise to a periodic conical whistler instability.

It is shown in [8] that the speed of the CME is slightly higher than the speed of the shock front. The increasing distance between the two can explain the smooth expansion of the main braid during the drift toward lower frequencies. In general, the shock front probably propagates at some angle to the magnetic field. In this case, the magnetic field and density of the shock front should have an oscillatory structure. This may be the origin of the presence of a number of other fragments of fiber braids and zebra stripes at higher frequencies, whose sources are located further behind the shock front.

The whistlers propagate in the direction of propagation of the shock front, but the group velocity of the whistlers cannot exceed $\sim 10^8$ cm/s, providing an explanation for the appreciably lower frequency-drift rate of the fibers within the main braid. Thus, these unusual braids of fibers are most likely a manifestation of the simultaneous propagation of a shock front and a CME in the corona with different speeds.

3.2. Event of July 28, 1999

The observations testify that new, hot loops rose before the two intervals of zebra-pattern structure, and that the radio sources were located above these loops (Fig. 2). It is obvious that the frequency bandwidth of the fine structure was determined by the

vertical size of these new flare loops in the corona. The radio sources were located above regions with northern magnetic polarity, and the left-circular polarization of the radio emission corresponds to the ordinary wave.

The inverse position of the absorption stripes in the zebra structure (from the high-frequency edge of the stripes of emission) over roughly ten minutes during the decay phase of the flare provides important information for theoretical models of the fine structure. A similar inverse position of fiber-burst absorption bands was considered in [13], where it was shown that, in this case, we observe radiation at the difference frequency $\omega_l - \omega_w = \omega_t$ as a result of the decay process $l \to t + w$. This variation in the interaction between plasma waves and whistlers is probably associated with variations in the magnetic-field gradient in the source, as are quite expected in regions of magnetic reconnection high in the corona.

The continuous transition between fiber bursts and zebra-pattern stripes (and vice versa) suggests a single origin for these two types of structure, especially since their main parameters are the same. In this connection, we note that the zebra-structure model of LaBelle *et al.* [16] is not able to explain the continuous transition between zebra structure and fiber bursts, since only the stability of a point source is considered. It is not clear what variations of the positions of the absorption stripes should be expected in this model, or what their origin would be.

3.3. Event of September 23, 1998

Analysis of all the available observational data for these event show that fine structure was observed simultaneously with the appearance of new, hot magnetic loops, and that the frequency bandwidth occupied by the fine structure in the spectrum (280–450 MHz) could realistically be determined by the extent of these new loops in the corona.

Again, the data demonstrate that the zebra structure consists not only of stripes of emission, but also of stripes with appreciable absorption, which are sometimes even dominant. For this reason, and also in connection with the simultaneous radiation from zebra structure, fiber bursts, and rapid pulsations, it is difficult to explain the zebra structure in this event with the new model of [16]. It is quite realistic to expect the excitation of electrostatic plasma waves and whistlers trapped by fast particles in new flare loops, but the formation of small inhomogeneities (solitons consisting of ion–acoustic waves) is not obvious (most importantly, the condition $T_e \gg T_i$), and is simply postulated by LaBelle *et al.* [16]. There also remain doubts about the applicability of the model of [16] to meter wavelengths, when the wavelength becomes comparable to the size of the inhomogeneities ($\lambda \sim L$), since $\lambda \ll L$ is a condition for applying geometrical optics to write the eiconal conditions (Eqs. (4) and (5) in [16]).

3.4. Event of October 25, 1994

In this brief event, the source of the zebra structure was located above an active region, as is shown in Fig. 4. A more detailed analysis of the X-ray frames (Yohkoh/SXT) is carried out in [22], where it is shown that there was additional brightening outside the main flare region as a result of magnetic reconnection involving the main flare loop and previously existing loops high in the corona.

The bandwidth of the zebra structure is probably determined by the distance in the corona between the magnetic-reconnection X point above a flare loop and a point high in the corona displaying shear between the rising flare loops and large-scale transequatorial loops, visible in the Yohkoh/SXT frames. Evidence supporting this picture is provided by the coincidence in the spectrum of the low-frequency boundary of the zebra structure and the frequency at which the drift of the type III outbursts ceases after about 10:08:35 UT (Fig. 4).

The spatial drift of the zebra-pattern structure at 164 MHz was toward the south, opposite to the drift of the type III outbursts. In our picture, this testifies that beams of fast electrons accelerated below in a flare current sheet (and responsible for the periodic type III outbursts) are reflected from a region with magnetic-field shear (where the new magnetic reconnection with the X point began). The reflected particles have a conical velocity distribution, generating plasma waves and whistlers, whose interactions give rise to the zebra structure at the corresponding frequencies.

However, the sign change of the spatial drift of the zebra structure that is correlated with the sign change of the frequency drift provides evidence that the spatial drift at a fixed frequency does not represent a real shift in the source position, but instead a shift in the energy maximum in the interval of heights associated with the radiation at that frequency (due to the velocity scatter for the rapid particles) and along the surface of equal density. Such a drift is quite plausible in a whistler model. The reflected particles should display conical anisotropy, and the whistlers should be excited in the anomalous Doppler resonance, when the particles and waves propagate in the same direction. In this case, the whistlers propagate downward with the group velocity, consistent with the positive frequency drift of the zebra-pattern stripes. The scattering of the whistlers on fast particles (quasi-linear effects) deforms the

distribution function: the longitudinal velocities are decreased while the transverse anisotropy grows, and the excitation of whistlers gradually switches to the normal Doppler resonance, when the particles and waves propagate in opposite directions and the group velocity of the whistlers gradually turns upward (this effect is considered in more detail in [11]). This switch in regime is completed at times of sign changes of the frequency drift of the zebra-pattern stripes, which coincide with times of sign changes of the spatial drift of the sources.

Even sharper shifts of the source center occurs at times corresponding to the transition to the zebra absorption stripes. In this case, no particle velocities can explain a shift by about 1.5 channels (each 3.2′) over one-third of a second (for example, at 10:08:41.3–10:08:41.7 UT), which yields a shift velocity of about $2c$, where c is the speed of light. In this case, we do not observe real motion, but instead a shift in the position of the maximum continuum radiation of the source, which indeed shifts by this amount (more than 4′) toward the southwest (above the maximum of the SXR flare in Fig. 4).

Thus, although the centers of the type III outbursts and zebra structure nearly coincide, the emission is radiated by different particles moving in different directions. In the case of the type III outbursts, these are beams of particles propagating from the acceleration region, which is the upper part of a flare current sheet at the height where $f_{Pe} \approx 450$ MHz; in the case of the zebra structure, these are particles reflected from a region with shear, at heights corresponding to the minimum frequency of the type III outbursts, where $f_{Pe} \approx 125$ MHz). The abrupt perturbation that partially stopped the frequency drift of the type III outbursts at 10:07:37–10:07:58 UT shows us the position in the corona of a new magnetic-reconnection X point (where $f_{Pe} \approx$ 170 MHz). At these heights, there was a partial capture of particles from the type III outburst beams, forming a new magnetic cloud (an island above the X point). The size of this new magnetic cloud between the X point and the magnetic-field shear determined the beginning of the frequency range of the zebra structure. Over a minute (10:08–10:09 UT), the whistlers gradually spread downward to levels where $f_{Pe} \approx 210$ MHz.

The large transverse size of the source suggests that the whistler instability developed over the entire width of a level of constant density above the active region, but the emission maximum could be appreciably shifted from the center of the continuum maximum along this level.

In our whistler model, each stripe of the zebra pattern is associated with an isolated whistler wave packet. The periodicity of the stripes most likely reflects periodicity in the instability due to the quasi-linear interactions between the whistlers and fast particles (periodicity in the deformations of the distribution functions). Periodicity in the injection of fast particles and the "bounces" of the particles in the magnetic trap will lead to additional periodicity in the observed phenomena. No obvious trap was observed in this event, and we can see a surprising coincidence in the number of type III outbursts at 10:08–10:09 UT (24) and the number of zebra-pattern stripes along the time axis. Quasi-linear effects lead to additional modulation along the zebra stripes. Such effects operate only when the particles and waves (whistlers) do not diverge in space. The smooth shift of the hump with the sign change of the frequency drift is due precisely to the diffusion of whistlers in rapid particles, when the time when the resonances are switched (see above) does not occur simultaneously at all frequencies (heights in the corona), but instead with a modest delay between frequencies, equal to the time for the diffusion at each level in the corona (for more detail, see [11]).

The double-plasma resonance model proposed in [26] to describe this phenomenon cannot explain the observed effects, even the number of zebra stripes in the observed frequency interval. For example, if we adopt, not some hypothetical distributions with a high density and magnetic field, but more realistic distributions, such as a double Newkirk model above the active region and a dipolar magnetic field whose scale height is much smaller than the density scale height, this model predicts only ten stripes in the observed frequency range of 135–170 MHz instead of the observed 18 stripes, with harmonic numbers s from 10 to 20, as was shown in [27]. Most importantly, instead of a smooth growth in the frequency separation between the stripes with increasing frequency (from 1.7 to 2.2 MHz), the model predicts a sharp growth from 2.5 to 7 MHz. Even larger discrepancies with the observations are obtained for other models (for example, density distributions that obey the barometric formula and magnetic fields that correspond to the model of [28]). Note that, while the field model of [26] is quite realistic (it was derived based on numerous radio observations), a barometric density distribution cannot be applied to magnetic loops with plasma parameters $\beta \ll 1$, since the barometric formula corresponds to a density distribution in a gravitational field with constant temperature and without a magnetic field.

This radio event was typical from the point of view of the activity in interplanetary space, where the groups of type III outbursts make a nearly smooth transition to a single large kilometer-scale type III outburst.

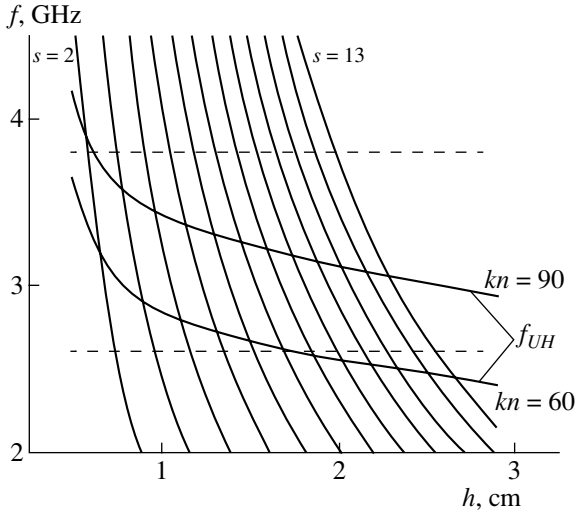

Fig. 7. Dependence of the plasma frequency and gyrofrequency in the magnetic-field model of Dulk and MacLean [28], which is derived from radio data ($B(\mathrm{G}) = 0.5(R/R_s - 1)^{-1.5}$, $1.02 \le R/R_s \le 10$), and a model with a Newkirk electron density multiplied by kn. The horizontal dashed lines delineate the range of the NAOC radio spectrograph, 2.6–3.8 GHz.

3.5. Centimeter Wavelengths (Events of October 29, 2000 and April 21, 2002)

Since the zebra-pattern structure and fiber bursts display similar spectral characteristics, we will consider both structures to be manifestations of whistlers in the radio source, due to their interactions with electrostatic plasma waves, $l + w \to t$, with both waves being excited by the same fast particles in hot flare loops, which have an anisotropic conical loss distribution. The computations of [29] show a growth in the whistler increment with the temperature of the background plasma in the flare region, with the growth in the cyclotron decay being compensated by the decrease in the whistler frequency with the maximum increment to $0.1\omega_{Be}$. The mean duration of a series of zebra structures and fiber bursts was about two seconds, and the propagation of whistlers without damping over this time places a constraint on the whistler increment of $< 0.5\ \mathrm{s}^{-1}$. This constraint can be used to estimate the magnetic-field strength in the region in which the flare is generated. Electron temperatures in the range 2–20 MK yield magnetic fields of $B = 125$–190 G for regions in which the electron density is $(8$–$18) \times 10^{10}\ \mathrm{cm}^{-3}$. These rough estimates coincide with estimates derived from the frequency-drift rate of the fiber bursts observed at the same time at these same frequencies, based on the formula $B = 15.43(\ln f - 3)^{-2} df/dt$ [30], which was obtained for a 60-fold Newkirk model and a whistler frequency of $\omega_w = 0.1\omega_B$. If we estimate the magnitude of B in the new model of LaBelle *et al.* [16], assuming that $\Delta f_s \sim 0.02 f_{Be}$, we obtain for $\Delta f_s = 80$ MHz implausibly high values $B \approx 1500$ G for regions close to the photosphere.

An alternative model based on the generation of plasma waves at the upper-hybrid frequency ω_{UH} under the conditions appropriate for the double plasma resonance was also considered. We can see from Fig. 7 that the main inadequacy of this model is associated with the increase in the frequency separation of the emission stripes Δf_s with increasing frequency: the model predicts an increase from 60 MHz at 2.7 GHz to ~450 MHz at 3.8 GHz, which is not generally observed. Usually, the frequency separation only slightly increases with frequency. In this connection, the example of the zebra structure shown in Fig. 5b is noteworthy, since it shows that the double-plasma-resonance model is not able to explain the presence of simultaneous emission in 34 stripes with virtually identical intensities in the range 2.6–3.8 GHz. At the same time, this situation is quite realistic in a whistler model, where strict periodicity of the stripes is specified by the whistler-excitation mechanism itself—fluctuations in the instability under the action of quasi-linear effects—independent of the models for the density and magnetic field in the corona.

The frequency profiles in Fig. 5b demonstrate rapid pulsations in the bright zebra-pattern stripes with a well defined period of 30 ms. Thus, these new observations support the conclusions of [31] that zebra structure at centimeter wavelengths always has fine spikelike structure, which can be explained in a natural way in whistler models for zebra structure.

Like the large number of zebra-pattern stripes, the stable appearance of series of zebra structures in a pulsating regime cannot be understood in the new model [16], since this model predicts a strong dependence for the frequency separation and the number of zebra stripes on the parameters of the inhomogeneities, while we observe only a very small growth in the frequency separation with increasing frequency. LaBelle *et al.* [16] can theoretically explain any parameters of zebra structure, but the parameters of inhomogeneities such as propagating ion–acoustic waves cannot remain so similar over a wide range of frequencies (interval of heights) over extended periods of time; i.e., the spectrum of the stripes would be expected to blend into the continuum.

Thus, new data on zebra structure and fiber bursts at centimeter wavelengths testifies that they have similar structures to those observed at meter wavelengths. A unified model for zebra structure and fiber bursts involving whistlers can yield realistic values for the magnetic-field strength $B \approx 160$ G at a plasma level of about 3 GHz. Using realistic dependences for

the electron density and magnetic field, the double-plasma-resonance model for zebra structure predicts a frequency dependence for the frequency separation between stripes that is much stronger than is observed.

4. CONCLUSION

We have analyzed several of the most recent zebra-structure events using a multi-faceted approach to study the flare processes based on all available new data from the Yohkoh, SOHO, and TRACE satellites. Zebra structure and fiber bursts are observed at frequencies from 20 to 6500 MHz. The radiation of electrostatic plasma waves at higher frequencies is probably suppressed in the dense flare plasma. The main relative spectral parameters and degree of circular polarization of zebra structure and fiber bursts are nearly identical. The relative width of the zebra-pattern stripes in emission varies very little with frequency ($\approx 0.003-0.005$); the radio emission corresponds to the ordinary mode.

New data on zebra structure and fiber bursts at centimeter wavelengths shows that they are similar to the corresponding structures at meter wavelengths. A unified model for zebra structure and fiber bursts involving whistlers can yield realistic values for the magnetic-field strength $B \approx 160$ G at a plasma level of about 3 GHz. Using realistic dependences for the electron density and magnetic field, the double-plasma-resonance model for zebra structure predicts a frequency dependence for the frequency separation between stripes that is much stronger than is observed.

Fine structure was observed simultaneous with the ascent into the corona of new, hot magnetic loops, and the frequency range occupied by the fine structure in the dynamical spectrum is determined by the extent of these new loops in the corona. The continuous transition from fiber bursts to zebra structure and vice versa testifies to a single nature for these two structures. All the main properties of the emission and absorption stripes can be explained in a model involving interactions between electrostatic plasma waves and whistlers. The mechanism at double plasma resonance can be invoked to account for the large-scale bands in the radiation whose duration is comparable to that of the entire event, as was shown, for example, in [10] for the EEL filament oscillating for two hours. A detailed analysis of the behavior of the radio sources corresponding to individual zebra stripes in event 1994-10-25 at meter wavelengths shows that analogous studies at centimeter wavelengths require new positional observations of the radio-source dynamics obtained on instruments such as the CCPT simultaneous with spectral observations.

ACKNOWLEDGMENTS

The Phoenix-2 spectral data were kindly presented by P. Messmer, and the ARTEMIS-IV data (Greece) by A. Hilaris. The author thanks K.L. Klein for the preparation and discussion of the Nancay radioheliograph data, M. Poquerusse for the ARTEMIS spectrograph data (Meudon), and P. Zlobec for the data from the Trieste Astronomical Observatory polarimeter. The SOHO and TRACE data were obtained from the SOHO and TRACE databases (EIT, LASCO), and the X-ray data from the Yohkoh/SXT database (ISAS, Japan). The author is grateful for support from the Paris Observatory in Meudon (the project CNRS 4994) and the Chinese Academy of Sciences (NAOC, Profs. Q. Fu and Y. Yan). This work was supported by the Russian Foundation for Basic Research (project no. 02-02-116201).

REFERENCES

1. C. Slottje, *Atlas of Fine Structures of Dynamic Spectra of Solar Type IV-dm and Some Type II Radio Bursts* (Utrech Observatory, 1981).
2. A. Krüger, *Introduction to Solar Radio Astronomy and Radio Physics* (Reidel, Dordrecht, 1979).
3. G. P. Chernov, L. V. Yasnov, Y. Yan, and Q. Fu, China Astron. Astrophys. **1**, 525 (2001).
4. J. Kuijpers, *Collective Wave-Particle Interactions in Solar Type IV Radio Sources* (Utrech Univ., 1975).
5. V. V. Zheleznyakov and E. Ya. Zlotnik, Solar Phys. **44**, 461 (1975).
6. L. Mollwo, Solar Phys. **116**, 323 (1988).
7. R. M. Winglee and G. A. Dulk, Astrophys. J. **307**, 808 (1986).
8. O. A. Mal'tseva and G. P. Chernov, Kinemat. Fiz. Neb. Tel **5**, 44 (1989).
9. G. P. Chernov, Astron. Zh. **66**, 1258 (1989) [Sov. Astron. **33**, 649 (1989)].
10. G. P. Chernov, A. K. Markeev, M. Poquerusse, *et al.*, Astron. Astrophys. **334**, 314 (1998).
11. G. P. Chernov, Astron. Zh. **73**, 614 (1996) [Astron. Rep. **40**, 561 (1996)].
12. G. P. Chernov, Astron. Zh. **53**, 1027 (1976) [Sov. Astron. **20**, 582 (1976)] .
13. G. P. Chernov, Astron. Zh. **67**, 126 (1990) [Sov. Astron. **34**, 66 (1990)].
14. V. G. Ledenev, M. Karlicky, Y. Yan, and Q. Fu, Solar Phys. **202**, 71 (2001).
15. M. Karlicky, M. Barta, K. Jiricka, *et al.*, Astron. Astrophys. **375**, 638 (2001).
16. J. LaBelle, R. A. Treumann, P. H. Yoon, and M. Karlicky, Astrophys. J. **593**, 1195 (2003).
17. H. S. Sawant, M. Karlicky, F. C. R. Fernandes, and J. R. Cecatto, Astron. Astrophys. **396**, 1015 (2002).
18. Y. Leblanc, G. A. Dulk, I. H. Cairns, and J.-L. Bougeret, J. Geophys. Res. **105**, 18215 (2000).

19. A. T. Altyntsev, R. A. Sych, V. V. Grechnev, *et al.*, Solar Phys. **206**, 155 (2002).
20. Z. Ning, Y. Yan, Q. Fu, and Q. Lu, Astron. Astrophys. (2002, in press).
21. H. Aurass, B. Vršnak, A. Hofmann, and V. Ruždjak, Solar Phys. **190**, 267 (1999).
22. P. K. Manoharan, L. van Driel-Gesztelyi, M. Pick, and P. Demoulin, Astrophys. J. **468**, L73 (1996).
23. G. P. Chernov, K.-L. Klein, P. Zlobec, and H. Aurass, Solar Phys. **155**, 373 (1994).
24. G. Mann, K. Baumgaertel, G. P. Chernov, and M. Karlicky, Solar Phys. **120**, 383 (1989).
25. G. P. Chernov, Pis'ma Astron. Zh. **23**, 949 (1997) [Astron. Lett. **23**, 827 (1997)].
26. V. V. Zaitsev and E. Ya. Zlotnik, in *Proceedings of the Scientific Conference "Active Processes in Sun and Stars"* (NIIRF SPbGU, St. Petersburg, 2002), p. 257 [in Russian].
27. G. P. Chernov, in *Proceedings of the Conference "Modern Problems of Solar and Stellar Activity"* (NIRFI, Nizhni Novgorod, 2003) [in Russian].
28. G. A. Dulk and D. J. McLean, Solar Phys. **57**, 279 (1978).
29. L. V. Yasnov, G. P. Chernov, Y. Yan, and Q. Fu, *Proceedings of the 10th European SPM, Solar Variability: from Core to Outer Frontiers, Prague, 2002*, ESA SP-506, 791 (2002).
30. O. Elgarøy, *Intermediate Drift Bursts* (Oslo Univ., Oslo, 1982), Rep. No. 53.
31. G. P. Chernov, Y. Yan, and Q. Fu, Astron. Astrophys. **406**, 1071 (2003).

Translated by D. Gabuzda